CORRELATION OF METEOSAT-3 ANOMALIES WITH DATA FROM THE SPACE ENVIRONMENT MONITOR

D.J.Rodgers[1*], A.J.Coates[1], A.D.Johnstone[1] and E.J.Daly[2]

[1] Mullard Space Science Laboratory, University College London, Holmbury St. Mary, Dorking, Surrey RH6 5NT, UK
[*] now at DERA, Farnborough, Hampshire GU14 OLX, UK
[2]ESA/ESTEC, 2200 AG Noordwijk, The Netherlands

ABSTRACT

Over 7 years, Meteosat-3 experienced 725 operational anomalies of suspected geophysical origin. These are compared to electrons in the energy range 43 to 300 keV measured by the on-board SEM-2 electron analyser. Many more anomalies occurred at times of high flux than could be accounted for by random statistics alone. Hence there is a strong linkage between electron flux and the anomalies.

Anomalies occurring at times of highest fluxes occurred almost exclusively between 3 and 9 hours local time. Those occurring at times of lowest fluxes occurred at any local time. Different mechanisms may produce these two types of anomaly. High flux are characterised by an intense burst of electrons virtually simultaneous with the anomaly. Low flux anomalies occur at moderate fluxes but after several days of enhanced fluxes. Deep-dielectric charging appears responsible for both these types of radiometer anomalies: sudden, intense high energy fluxes causing some discharges while others being due to a slow flux build-up.

1. INTRODUCTION

Meteosat-3 was launched in 1988 into geostationary orbit. Between June 1988 and October 1995, when it was turned off, it experienced 725 operational anomalies had no apparent on-board origins. This study was carried out to see what parameters measured by the on-board Space Environment Monitor (SEM-2), if any, are associated with anomalies and what they imply for the mechanisms by which they occur. Some results from the first 18 months of Meteosat-3 operation have already been described (Ref. 1) and a similar correlation has been carried out for the 14 months of the CRRES spacecraft (Ref. 2). Here we present results based on the complete 7-year Meteosat-3 database.

The placing of particle instruments on Meteosat spacecraft was considered important after Meteosat-1, launched in 1977, exhibited a number of unexplained anomalies. Anomalies in geostationary orbit are generally thought to be the result of one of two mechanisms:

- Surface charging: the charging of spacecraft surfaces and subsequent discharge (Refs. 3,4,5). This charging is caused principally by electrons in the energy range 10keV to 20keV. In the geostationary environment, electrons are generally characteristic of the plasma sheet with typical temperature 1keV (Ref. 6). At times of increased magnetospheric activity, fluxes rise and temperatures may increase to about 10keV.
- Deep-dielectric charging: charge build-up within dielectric materials and subsequent discharge (Refs. 7,8). High energy electrons (>1MeV) characteristic of the outer radiation belt (Ref. 9) are involved and charge maybe stored over time-scales of a week or longer (Ref. 10).

The direct interaction of radiation particles with electronic components to produce single-event upsets, is not common in this region because it is far outside the proton belt and the electrons can be excluded by moderate shielding.

Charging of parts of the spacecraft surface and the resulting discharge were initially suspected to be the cause of the Meteosat-1 anomalies and Frezet et al. (Ref. 3) showed that large surface charging levels could occur. The next Meteosat satellite, Meteosat-2, carried a space environment monitor (SEM-1) (Ref. 11) that measured electrons from 30eV to 20keV. This found that surface charging events were common but not correlated with the anomalies. Because of this, Meteosat-3 was equipped with SEM-2 (Ref. 12) that looked at higher electron energies (43-300 keV) to see if the anomalies were related to these higher energy fluxes.

Previous studies (Refs. 12,13) have shown the existence of a correlation between Meteosat-3 anomaly occurrence and the daily energetic electron flux. In addition there was a strong seasonal variation in the rate of occurrence of anomalies with a large peak at the spring equinox. Such variations may indicate a dependence on spacecraft eclipses, on the solar aspect angle or on seasonal magnetospheric variations. The radiometer was the on-board system most prone to anomalies on the spin-stabilised satellite and was recessed deeply inside the spacecraft (Figure 1). Because of this, its solar illumination varied with the seasonally varying solar aspect angle.

The fact that the sensor was on the same spacecraft provides an excellent opportunity for correlation studies which are normally hampered by having anomalies and sensor on different spacecraft. We present a detailed analysis of the anomalies and correlations with electron fluxes.

2. DESCRIPTION OF SEM-2 DATA

SEM-2 was an array of five surface barrier detector-collimator systems .The detectors were arranged in a fan with each set at a different angle to the spacecraft spin axis to give five polar angle bins - 30°, 60°, 90°, 120° and 150°. The instrument discriminated the height of the pulse, dividing the energy range into five bins (Table 1). The upper energy limit of 300keV corresponds to the most energetic electron that can be stopped within the detector. Particles with higher energy will pass through without depositing all their energy and will appear in this energy band. From the raw data, a 'Spectral Index' γ is calculated as a fit to a power law spectrum, where $Flux(E) \propto E^{\gamma}$.

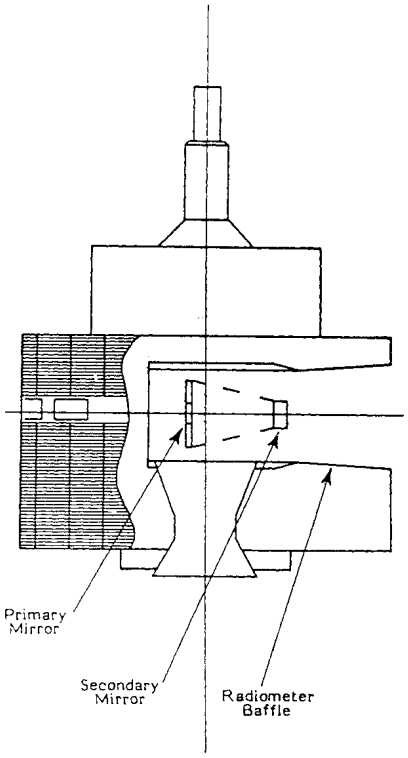

Figure 1. Schematic diagram of a Meteosat satellite showing the recessed radiometer baffle and mirror (Ref. 9).

Energy Bin	E_{LOWER}	E_{UPPER}
1	42.9 keV	59.4 keV
2	59.4 keV	90.7 keV
3	90.7 keV	134.9 keV
4	134.9 keV	201.8 keV
5	201.8 keV	300 keV

Table 1: SEM-2 Energy bin ranges

3. CHARACTERISTICS OF THE ANOMALIES

Anomalies are simply unexpected spacecraft behaviour that cannot be explained as software or command errors. There is no reason to expect that different kinds of anomalies should have been produced by the same processes. The largest group (486) of anomalies seen on Meteosat-3 and the most statistically significant, involved the Radiometer. This experienced many unexpected stoppages and position jumps.

Fig. 2 shows the number of Radiometer anomalies in each month between June 1988 and November 1995 and the average flux at 43-300KeV. The duty cycle of the radiometer was not always constant and has a strong effect on the rate of anomalies. Hatched lines show periods of greater than a month when the radiometer was off for almost all of the time. Periods when SEM-2 data are unavailable are shown in the same way. Periods of increased anomalies generally coincide with periods of increased flux. However, there is a stronger correlation with 'injection events', here defined as peaks in the 43-300KeV flux exceeding 3.5×10^4 cm^{-2} sr^{-1} s^{-1} keV^{-1}. These peaks occur when electrons are injected into the inner magnetosphere by processes taking place in the tail. Monthly averages of the same data over the 7-year database (Figure 3) shows strong increases in anomaly occurrence near the equinoxes. Similar increases are seen in the flux but are strongest in the injection events.

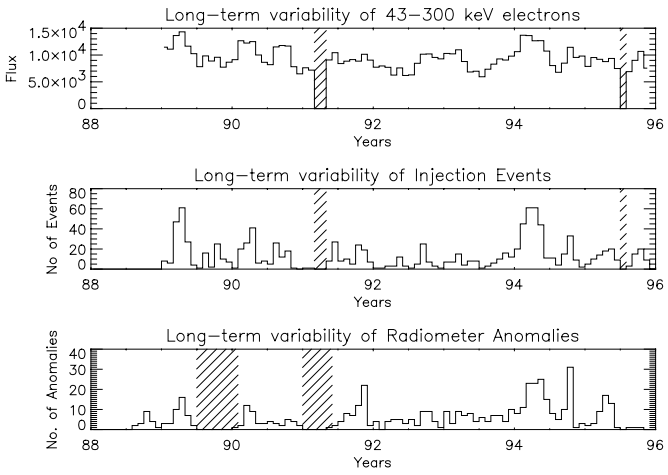

Figure 2. Total flux in energy range 43-300KeV, and number of injection events and anomalies in each month of the Meteosat-3 data set.

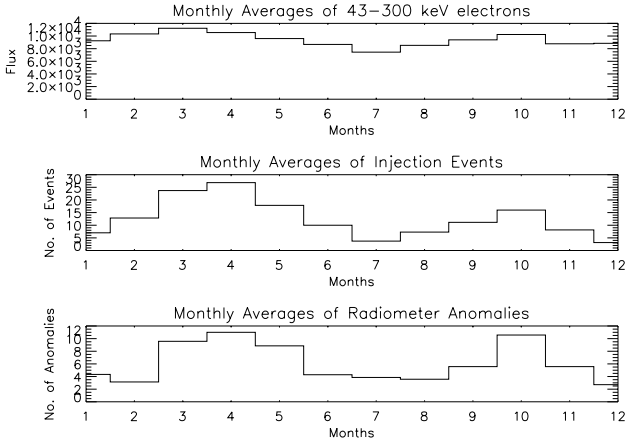

Figure 3. Monthly averages of total flux in energy range 43-300keV and number of injection events and anomalies.

Figure 4 shows the distribution of radiometer and non-radiometer anomalies in local time. There is a significant peak in occurrence of radiometer anomalies between 3 and 6 hours compared to other times. For the non-radiometer anomalies, there was no noticeable local time dependence.

If the Radiometer anomalies are indeed associated with electrons in the SEM-2 energy range then local time and seasonal dependence of anomalies is to be expected. However the situation may be complicated because other factors that may influence the electrical properties of the satellite, such as illumination and temperature, also vary diurnally and seasonally. Because there are sufficient numbers of them for statistical analysis and their local time dependence suggests a geophysical origin, the radiometer anomalies alone have been studied further.

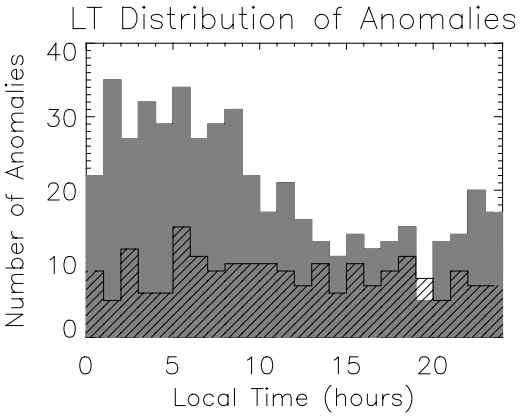

Figure 4. Radiometer (shaded) and non-radiometer (striped) anomalies binned according to local time.

4. DETAILED COMPARISON

Our comparisons comprise mainly analyses of frequency of anomaly occurrence and 'summed epoch' plots, in which the time-histories of a parameter for an extended period around the anomaly are accumulated, giving the average behaviour of the parameter around the time of the anomaly. Using both techniques means that correlations can be identified if they depend only on the instantaneous value of a certain parameter, or if they require the parameter to be disturbed for some time.

4.1 Anomaly Frequency Correlations

Figure 5 shows the number of anomalies, binned according to the instantaneous total flux above 43keV. The strongest peak was at 11000 cm^{-2} sr^{-1} s^{-1} keV^{-1} but the anomalies were scattered widely from zero to 50000 cm^{-2} sr^{-1} s^{-1} keV^{-1}. However, to assess whether the total flux and the anomalies are related we must add information about the likelihood of the flux levels. The second panel shows that the total flux itself was much more commonly around 6000 cm^{-2} sr^{-1} s^{-1} keV^{-1}. When the anomaly frequency is normalised by dividing by the total flux frequency (third panel), it is clear that the anomalies occur preferentially at times of higher flux.

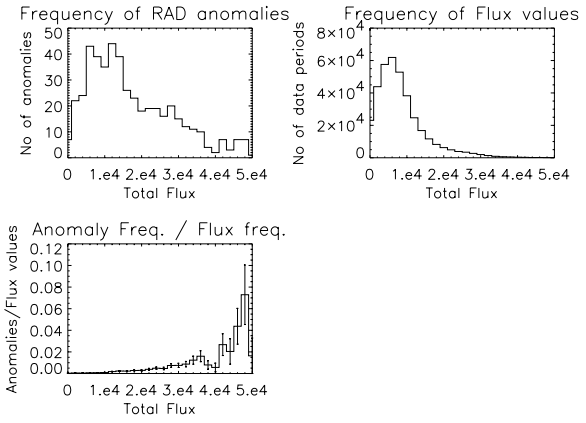

Figure 5. Top Left: Radiometer anomaly occurrence binned according to the instantaneous value of the total flux. Top Right: Frequency of occurrence of each total flux value. Bottom Left: Radiometer anomaly occurrence normalized by the frequency of total flux occurrence. Error bars show the increasing error at higher flux values.

Fig. 6 shows the same frequency analysis of the anomalies and data, binned according to spectral index γ. The resulting anomaly/flux frequency ratio is fairly flat over most of the range but showed a dearth of anomalies at the most negative spectral index values and an excess of anomalies at the least negative values. This relationship is not as strong as the total flux, but it implies that flux at the top of the SEM-2 energy range or higher is most important in causing anomalies.

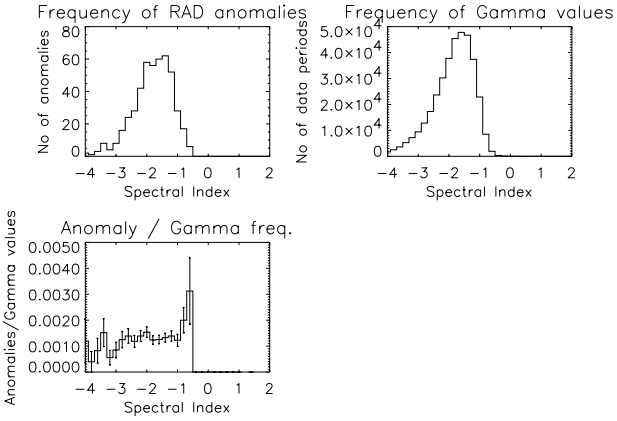

Figure 6. Top Left: Radiometer anomaly occurrence binned according to the instantaneous value of the Spectral Index γ Top Right: Frequency of occurrence of each χ value. Bottom Left: Radiometer anomaly occurrence normalised by the frequency of γ occurrence.

4.2 High-Flux and Low-Flux Anomalies

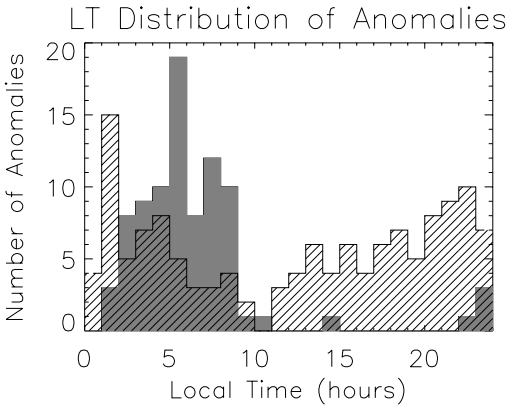

Figure 8. Anomalies with flux >30000 (shaded) and <10000 (striped) binned according to local time.

Although Fig. 5 shows that anomalies occur preferentially during high electron fluxes, only 87 out of 480, for which there were SEM-2 data, occurred with over 30000 cm^{-2} sr^{-1} s^{-1} keV^{-1} and a large number still occurred at low flux levels. Some even occurred well below the mode flux of 6000 cm^{-2} sr^{-1} s^{-1}. Hence instantaneous flux cannot be the only factor. To investigate any differences between the high- and low-flux anomalies, the anomalies with fluxes below 10000 and above 30000 cm^{-2} sr^{-1} s^{-1} keV^{-1} were analysed separately to see if they had more differences than flux alone. Figure 8 shows the

local time distribution for these groups. The >30000 group peaks strongly between 3 and 9 hours local time. This is when injection events above $3.5x10^4$ cm^{-2} sr^{-1} s^{-1} keV^{-1} are most common, as is shown in figure 9. Choosing a different flux threshold to define the injection events would modify the local time distribution of the injection events, since these events decay as they propagate eastwards from the tail sector.

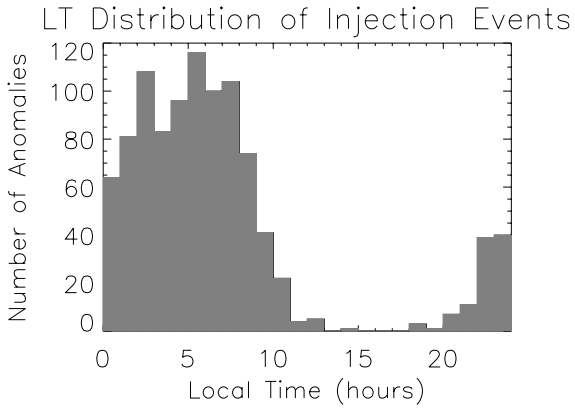

Figure 9. Injection Events binned according to local time.

The <10000 group is more widely distributed and anomalies occur even where there are few injection events.

The seasonal distribution of the high- and low-flux events is shown in figure 10. High flux events occur mainly at the equinoxes when injection events are common but the low-flux events are more evenly spread.

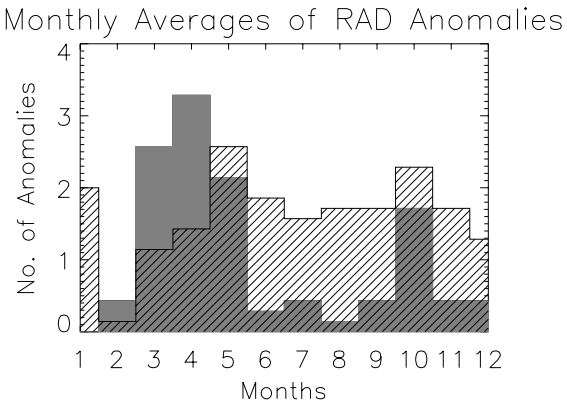

Figure 10. Anomalies with flux >30000 (shaded) and <10000 (striped) binned according to month.

There is thus strong circumstantial evidence, linking some of the anomalies with injection events. Other anomalies appear to have no correlation with instantaneous flux levels.

4.3 Summed Epoch Analysis

By averaging the time history of the electron flux relative to the time of each anomaly, a general view can be obtained as to what environment changes precede a typical anomaly. Here, we have concentrated on electron flux.

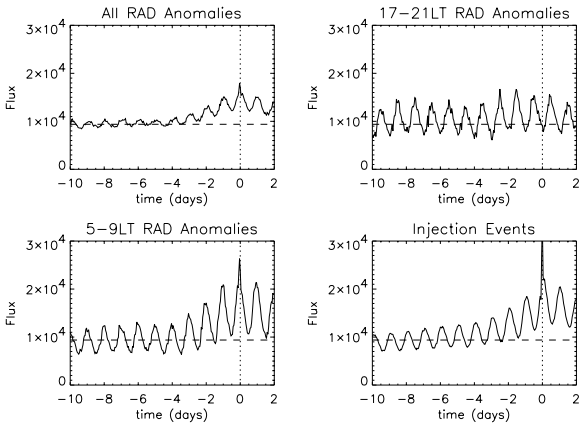

Figure 11. Summed epoch plot of total flux between 10 days before and 2 days after: all anomalies; 5-9 hours local time anomalies; injection events with flux>35000 cm^{-2} sr^{-1} s^{-1} keV^{-1}; and 17-21 hours local time anomalies.

Figure 11 shows the average time history of total flux (43<E<300keV), for 10 days before and 2 days after four classes of events: All radiometer anomalies; all 5-9 hours LT radiometer anomalies; all 17-21 hours LT radiometer anomalies; and all injection events. The two groups of anomalies differentiated by local times 12 hours apart represent high-flux anomalies apparently associated with injection events and low-flux anomalies which are apparently not. The dashed horizontal line is the mean over the entire database and the dotted vertical line shows the time of the anomaly or injection event.

The top-left panel, showing the sum over all radiometer anomalies, indicates that ten days before an anomaly, the flux is approximately at the mean level. Starting about 3 days before the anomaly, the flux rises, reaching a peak of 1.9 times the mean flux around the time of the anomaly. This is clear evidence that a significant proportion of the anomalies are really linked to instantaneous electron flux.

The average total flux around the radiometer anomalies which took place between 5 and 9 hours local time, the bottom-left panel, shows a stronger diurnal variation but a similar build-up period of about 3 days. There is a particularly strong flux peak, reaching 2.8 times the mean, immediately before an anomaly occurs. This shows that anomalies in this local time bin are directly caused by the high fluxes in injection events.

The bottom-right panel shows that the time-history before injection events has a similar 3-day build-up. This simply means that injection events tend to occur repeatedly over a period of a few days and the apparent build-up before the anomalies may not result from a characteristic charging time.

The top right panel treats 17-21 hours local time anomalies in the same way. These anomalies occur at a low-point in the diurnal flux variation. Hence it is clear that they are not associated with injection events occurring at abnormal local times. They may however be associated with the small excess in flux seen in the 3 days before the event and perhaps longer.

Figure 12 shows, in higher time resolution, a log-linear plot of fluxes in all 5 energy bins in the three hours before and after the 5-9 hours LT anomalies. There is a simultaneous peak in

all energies except the lowest, in the ten-minute time bin centred on the anomaly. The increased flux is not symmetrical about the time of the anomaly, being higher before the anomaly than after.

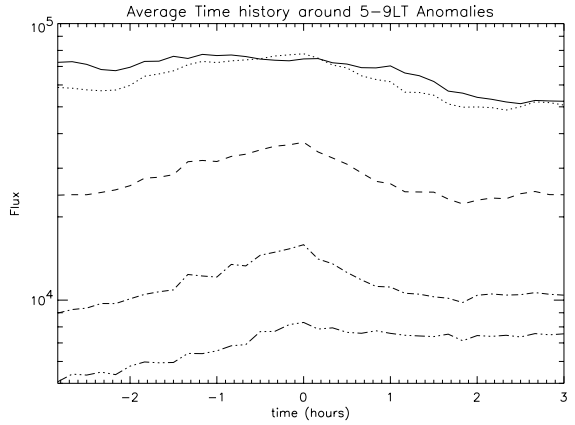

Figure 12. Summed epoch plot of flux in the 3 hours before and after anomalies in the 5-9 hours local time range. Solid line 43-60keV, dotted line 60-91keV, dashed line 91-135-keV, dashed and dotted line 135-202keV, dash and three dots 202-300keV.

4.4 Energy Spectra Associated with Anomalies

In order to see if one particular part of the SEM-2 energy range is more important than others, the average flux in each of the five energy bins was found at the time of the 5-9 hours LT anomalies. At these times, all energy bins are enhanced compared with the average level. The data were divided by the mean of the complete data set to remove the effects of their different average levels. This enhancement over the mean level is tabulated in Table 2.

Energy (keV)	Anomaly Flux / Mean Flux	High Flux / Mean Flux	Anomaly Flux / High Flux
43-59	2.21	2.77	0.80
59-91	3.10	3.83	0.81
91-135	3.52	3.94	0.89
135-202	3.62	3.25	1.11
202-300	2.61	2.14	1.22

Table 2. Average peak flux: associated with 5-9 hours LT anomalies; during injection events: and the ratio between the two.

The highest enhancement occurred in the 135-202keV energy bin. At first glance this suggests that these medium energy electrons are most strongly associated with anomalies. However, the spectrum changes anyway as flux levels rise and this effect must be taken into account. The average spectrum was found for periods of high total flux. The definition of high flux was >25000 cm^{-2} sr^{-1} s^{-1} keV^{-1}, which was near the mean flux for the 5-9 hours LT anomalies. The ratio of this spectrum to the mean spectrum is tabulated in table 2. The highest enhancement also occurs in the middle energy levels. It is only by taking the ratio of the enhancement during the anomalies and the enhancement at high flux times, that the difference between anomaly periods and other high flux periods becomes clear. This is shown in the final column of table 3 and shows that anomaly periods are particularly associated with increases at the highest energies.

The average spectrum of the previous maximum before the 17-21 hours LT anomalies was also examined. This too showed the largest increase in the highest energy bin compared to the high-flux periods.

5. DISCUSSION

Electrons (43-59keV) most expected to be associated with surface charging did not peak significantly at the time of the anomalies in the 5-9 hours local time range. The electrons that appear most closely associated with these anomalies are at the upper energy channel of the SEM-2 instrument. Electrons with such energies can penetrate dielectrics to deposit charge although they would be stopped by moderate levels of shielding. A 300keV electron can penetrate about 1mm of polythene (Ref. 14). Since the highest SEM-2 energy bin also contains electrons with energy greater than 300keV greater penetration depths are possible. Hence the electron energies are in the right range to cause deep-dielectric charging. Electrons with these energies are not usually associated with surface charging because their fluxes are too low. The fact that fluxes are higher just before these anomalies than after, points to the electrons building up over a brief period (~1 hour) before a discharge causes the anomaly. Hence, deep-dielectric charging seems the most likely mechanism. These anomalies can occur in rapid succession: 16 of the 121 radiometer anomalies in the 5-9 hours local time range occurred in the same 3-hour time bin as the previous radiometer anomaly.

Other anomalies, particularly those that occur in the 17-21 hours LT range, occur after a long flux build-up even though they occur at times of low instantaneous flux. This can only be the result of deep-dielectric charging. Here the charge build-up period must be at least 12 hours and is probably several days. There were no repeated anomalies in the same 3-hour period amongst the 45 anomalies in the 17-21 hours range and only 3 within 2 days.

Two different processes are proposed to explain these two classes of anomalies:

– If there is a sudden large burst of energetic electron flux, this can accumulate internal charge very rapidly and produce a discharge. No long build-up of charge appears necessary. This occurs most often in the morning sector where such bursts of flux are most commonly found.
– If there are generally high flux levels but an intense burst of flux does not happen then the flux accumulates gradually for several days. After this time, the discharge occurs anyway, possibly in response to some external trigger. However, there is nothing in the SEM-2 data to say what this trigger could be.

The identification of deep-dielectric charging as the likely mechanism is in agreement with the conclusions of the CRRES (Ref. 2) study, although on that spacecraft almost all anomalies occurred far inside geostationary orbit and the spacecraft design was very different.

It is possible that high-flux and low-flux anomalies result from discharges at different parts of the spacecraft. For example,

some discharges may take place on a surface that has extremely low conductivity to the rest of the spacecraft, allowing charges to build up over several days. At other sites, where conductivity is higher, a brief intense burst of flux may be required.

Because these anomalies affect the radiometer it is natural to suppose that the relevant part or parts of the spacecraft interacting with the plasma may be inside the radiometer cavity. However, there was no evidence of this in the data. In work not presented here, no increase in anomalies was found to occur when the axis of symmetry of the electron distribution aligned with the spacecraft axis - an orientation which would usually permit more electrons to enter the radiometer cavity. Hence, from the SEM-2 data there is no evidence that the site of the charging is within the radiometer cavity.

As was seen in an earlier study (Ref. 12) there was a seasonal dependence to the anomalies. This reflects the seasonal dependence of injection events but shadowing of the spacecraft may also be a factor. Spring and autumn equinoxes are periods when the sun shone directly into the cavity. This would be expected to reduce surface charging effects (as was seen on Meteosat-2 (Ref. 11)) but would have a less direct effect on deep dielectric charging. It could affect the probability of discharges occurring by keeping the surface near zero potential.

6. CONCLUSIONS

The main conclusions of this study are as follows.

- On average, the total electron flux shows significant enhancement at the time a radiometer anomaly occurs indicating a clear correlation between electron flux and anomaly occurrence. The strongest correlation occurs for fluxes above 200keV.
- Many anomalies can be directly linked to 'injection events'. These anomalies occurred preferentially between 3 and 9 hours local time and around the equinoxes, when injection events are more common.
- Some anomalies occurred when instantaneous fluxes were average or low. However, these occurred when fluxes had been high for 3 or more days. These were seen at all local times.
- The two types of anomalies have the following typical features:

	'High Flux' Anomaly	'Low Flux' Anomaly
Local Time	3 to 9 hours	All local times
Charging period	probably > 3 hours	probably several days
Electron energy	>200keV	>200keV
'Trigger'	Burst of high flux	unknown

- From the energy of the associated electrons (>200keV) and time-lag between peak flux and the anomaly, it is likely that deep-dielectric charging is occurring in both cases.
- The radiometer cavity cannot be confirmed as the site of the discharge.

A general conclusion is that the geostationaty environment continues to be hostile for spacecraft and the usefulness of including small, inexpensive environment monitoring instruments on spacecraft is evident.

Acknowledgements

We thank T.A.Fritz and R.D. Belian (Los Alamos National Laboratory) who supplied the detectors for SEM-2 and J.Aasted and R.Salisbury (ESA/ESTEC) who were responsible for including the SEM-2 instrument on Meteosat-3. Data analysis was supported by ESA contract 7879/88/F/TB.

REFERENCES

1 Rodgers D.J. 'Correlation of Meteosat-3 Anomalies with Data from the Spacecraft Environment Monitor', ESTEC working paper 1620, 1991

2 Violet M.D and Frederickson A.R. 'Spacecraft Anomalies on the CRRES Satellite Correlated with the Environment and Insulator Samples'', IEEE Trans.Nucl.Sci. Vol. NS-40, pp.1512-1520, 1993

3 Frezet M., E.J.Daly, J.P.Granger and J.Hamelin 'Assessment of Electrostatic Charging of Satellites in the Geostationary Environment', ESA Journal, Vol. 13, 1989, pp.89-116.

4 Garret H.B. 'Spacecraft Charging: A Review', Space Systems and Their Interactions with Earth's Space Environment} 1st Ed. H.B.Garrett, Prog. Astronaut. Aeronaut, 71}, AIAA, 1980, p. 167.

5 Garrett H.B. 'The Charging of Spacecraft Surfaces', Handbook of Geophysics and the Space Environment, Ed. A.S.Jursa, AFGL, Hanscom AFB, MA, 1985, pp.7-1 to 7-37

6 Burke W.J., D.A.Hardy and R.P.Vancour 'Magnetospheric and High Latitude Ionospheric Electrodynamics', Handbook of Geophysics and the Space Environment, Ed. A.S. Jursa, AFGL, Hanscom AFB, MA, 1985, pp. 8-1 to 8-30.

7 Meulenberg A.Jr. 'Evidence for a New Discharge Mechanism for Dielectrics in a Plasma, Spacecraft Charging in Magnetospheric Plasma, Prog. Astronaut. Aeronaut., Ed. A.Rosen, Vol. 47, MIT Press, 1976, p.237.

8 Frederickson A.R. Electric Fields in Irradiated Dielectrics, Spacecraft Charging Technology - 1978, Ed. R.C.Finke and C.P.Pike, NASA CP-2071/AFGL TR-79-0082, Hanscom AFB, MA, 1977, pp. 554-569.

9 Daly E.J. The Evaluation of Space Radiation Environments for ESA Projects, ESA Journal, Vol. 12, 1988, pp. 229-247.

10 Frederickson A.R. Bulk Charging and Breakdown in Electron Irradiated Polymers, Spacecraft Charging Technology 1980, pp. 33-51, 1981,

11 Johnstone A.D., G.L.Wrenn, H.E.Huckle and R.F.Scott 'Meteosat-F2 Spacecraft Charging Monitors', ESTEC, Noordwijk, The Netherlands, 'Final Report contract nos. 4715/81/F/CG, 5911/84/F/CG, 1985

12 Coates A.J., A.D.Johnstone, D.J.Rodgers and H.E.Huckle 'Meteosat-P2 Technical Assistance', ESTEC, Noordwijk, The Netherlands, Final Report contract no. 7879/88/F/TB, 1989

13 Coates A.J., A.D.Johnstone, D.J.Rodgers, G.L.Wrenn and A.J.Sims Quest for the Source of the Meteosat Anomalies Proc. Spacecraft Charging Technology Conference, 1989, Naval Postgraduate School, pp.120-146, 1991

14 Powers W.L., B.F.Adams and G.T.Inouye 'Electron Penetration of Spacecraft Thermal Insulation, Spacecraft Charging Technology 1980, AFGL-TR-81-0270, Hanscom AFB, MA, 1981, pp. 86-95.